Chapter 1

Introduction

1.1 Classification of Phase Transitions

The study of phase transitions is one of the well developed branches of condensed matter physics [1]. A phase transition occurs when the properties of a material undergo a change due to changes in temperature or pressure. Examples of phase transitions are melting of a solid and boiling of a liquid. Transitions can also occur between phases in the solid state. An example of such a transition is the transformation of a ferromagnetic substance like Iron or Nickel into a paramagnetic state. Elements like Iron and Nickel, possess permanent magnetic moments, which align spontaneously, below the transition temperature known as the Curie temperature. As the temperature of the material is increased, the degree of this alignment decreases continuously until at the Curie temperature it becomes zero.

The stability of a phase is discussed in terms of the Gibbs free energy (G) of the system.

$$G = U - TS + PV \tag{1.1}$$

Where U = Internal energy of the system

T = Temperature

S = Entropy

P = Pressure

V = Volume

In the presence of a magnetic field, a term MH is added to the Gibbs free energy .

For an infinitesimal , reversible transition,

$$dG = dU - TdS - SdT + PdV + VdP \tag{1.2}$$

Using the first law of thermodynamics

$$TdS = dU + PdV \tag{1.3}$$

Therefore

$$dG = -SdT + VdP \tag{1.4}$$

Since at the transition point the system is in thermodynamic equilibrium, $dT = dP = 0$ Hence $dG = 0$ or G = constant at the transition.

Even though the Gibbs free energy is a constant during a phase transition the derivatives of the free energy like volume, entropy, specific heat, compressibility or susceptibility can show a discontinuity at the transition point.

The discontinuities in the various thermodynamic quantities is the basis for a system of classifying phase transitions. According to this system of classification, propounded by Ehrenfest [2], phase transitions are classified according to the lowest derivative of the free energy which shows a discontinuity. If the first derivative of the free energy i.e, either the volume or the entropy shows a discontinuity at the transition temperature , then it is known as a first order transition. Examples of first order transitions are melting of a solid and boiling of a liquid.

If the second derivative of the free energy i.e, one of the response functions like specific heat, susceptibility etc show a discontinuity, it is known as a second order transition. An example of a second order transition is the transition from the normal metallic state to the superconducting state in zero magnetic field.

This system of classification fails for certain transitions , like the case of the Curie point transition in uniaxial ferromagnets, where the second derivatives of the free energy diverge to infinity. Hence it is difficult to see whether there is a discontinuity or not. The modern classification of phase transitions due to Fisher, takes this into account and broadly classifies phase transitions into discontinuous or continuous transitions.

1.2 Theories of Phase Transitions

In this thesis we will concentrate on magnetic transitions. The earliest theory for the ferromagnetic to paramagnetic transition was given by Weiss in 1908. According

to this theory each atom is assumed to have a localized magnetic moment which interacts with an average 'molecular' magnetic field due to all the other moments.

L.D.Landau, in 1944, generalized all the previous theories of phase transitions and gave a general formulation which is known as Landau's Mean field theory. Landau used a concept known as the order parameter, first introduced by Felix Bloch. The order parameter has a non-zero value below the transition temperature and is zero above the transition temperature. The order parameter varies discontinuously in a first order transition and goes continuously to zero for a continuous transition.

The main idea in Landau theory is that the free energy of the system can be expanded as a series in the order parameter [3].

$$G = G_0 + aM^2 + bM^4 + ... \tag{1.5}$$

Where G_o is a constant. Eq. 1.5 is written under the assumption that the value of the order parameter is small near the transition temperature. Hence it should be valid for continuous phase transitions. The most general expression for the free energy would involve all possible powers of M. However it can be proved from simple symmetry considerations that most of them should be absent. Since the free energy is a minimum at equilibrium, $dG/dM = 0$. From this condition it is seen that the coefficient of the linear term is zero. For magnetic systems, there are additional constraints on Free energy from the symmetry consideration that $G(M) = \mathrm{G}(-\mathrm{M})$. This is because the free energy should be the same , irrespective of the direction of magnetization. Therefore terms containing odd powers of M are absent from the expression for the free energy. In case the symmetry permits the presence of a term containing M^3, it can be shown that this leads to a first order transition. A first order transition is also possible without the M^3 term, if 'b' becomes negative. To ensure stability, a term containing M^6 has to be included in Eq. 1.5. For such a system, the transition is first order when $\mathrm{b} < 0$, and second order when $\mathrm{b} > 0$. The point where $\mathrm{a} = \mathrm{b} = 0$ is known as a 'tricritical point'. This shows that magnetic transitions can also be first order under certain circumstances

The following form is usually assumed for the constant 'a'

$$a = a_o(T - T_c) \tag{1.6}$$

It is obvious from the above equation that 'a' has a negative sign for $\mathrm{T} < T_c$ and a positive sign for $\mathrm{T} > T_c$. A and b are constants independent of temperature, except under the circumstances discussed earlier.

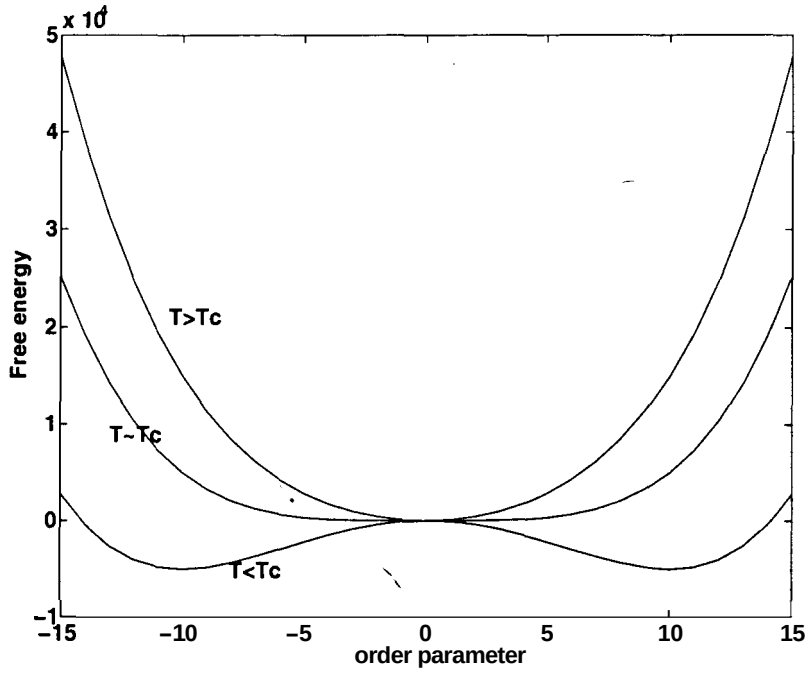

Figure 1.1: The Landau free energy as a function of the order parameter at different temperatures

---

The equilibrium configuration of a system is found by minimizing the free energy with respect to variations in the order parameter. Therefore the condition for equilibrium is that $dG/dM = 0$, i.e,

$$\frac{dG}{dM} = 2aM + 4bM^3 = 0 \tag{1.7}$$

This equation has the solution $M = 0$ or

$$M = \left(\frac{a_o(T_c - T)}{2b}\right)^{1/2} \tag{1.8}$$

Therefore according to Landau theory the order parameter varies as $(T-T_c)^{1/2}$. The free energy has been plotted as a function of the order parameter for different values of temperature in Fig. 1.1.

Below T_c, the free energy has two minima, corresponding to the two equivalent directions of magnetization, $-M$ and M. Above T_c, there is only one minima at $M = 0$. As T approaches T_c from the low temperature side, the two minima approach each other and coalesce to a single point for $T = T_c$. Near T_c, the free energy curve is almost flat around the minima $(\mathrm{M} = 0)$. This brings into focus why fluctu-

ations in the order parameter are important especially near T_c. All thermodynamic quantities are usually macroscopic quantities which are obtained by averaging over macroscopic dimensions. There could be fluctuations on a microscopic length scale. These fluctuations in the order parameter cost energy which depends on the size of the fluctuation. The energy for the fluctuations are supplied by the Auctuations in the thermal energy of the system. The effect of fluctuations are neglected in the Landau theory based on Eq. 1.5.

To illustrate the effects of these fluctuations consider the free energy curve for a temperature T slightly above T_c. The average value of the order parameter is 0, however fluctuations about this average value do not cost much energy as the curve is almost flat. Hence the energy of the system is almost the same for a range of M values about the average. This situation is no longer true far away from the transition point, where the curvature at the minima of the energy is quite large, leading to a large energy change for the same amount of fluctuation in the order parameter.

From the above discussion it emerges that a large number of states have the same energy, when the system is near the transition point. This in turn means that a long time is required for the system to attain equilibrium, as it has to sample all the available states. This phenomenon is known as 'critical slowing' down of the system near the transition point. The 'critical slowing down' of the system creates some experimental problems when a thermodynamic property has to be measured, as the experimental time-scales diverge near the transition point.

The Landau theory ,like the Weiss theory of ferromagnetism, predicts a discontinuity (ΔC_v) in the specific heat

$$\Delta C_v = \frac{a_o^2 T_c}{8b} \tag{1.9}$$

Experimental studies on ferromagnetic materials showed that while the mean field theories were successful in predicting the behaviour far from the transition temperature, it fails quite dramatically in its prediction near the transition temperature. While the mean field theories predict only a discontinuity in the specific heat, ferromagnetic materials like Iron and Nickel show a finite cusp and some fluids show an infinite divergence. The experimentally observed specific heat variation can be fitted to a power-law of the form

$$C_v = (A/\alpha)(T - T_c)^{-\alpha} + B \tag{1.10}$$

Where T_c is the transition temperature and a is known as the critical exponent.

The failure of the mean field theories to predict the behaviour near the transition point is related to the fact that the theory assumes an average field throughout the sample and neglects short-range interactions. The Ginzburg-Landau formulation tries to rectify this defect by taking fluctuations into account.

The Ginzburg - Landau free energy is given by

$$G = G_o + c|\nabla M|^2 + aM^2 + bM^4 \tag{1.11}$$

The renormalization group theory of K.G.Wilson [4] uses this free energy to calculate the variation of thermodynamic quantities near the critical temperature. It gives values for the critical exponents which agree quite well with the experimentally observed values of the critical exponents.

An important triumph of the renormalization group theory is the explanation of the phenomenon of 'universality', i.e, the explanation of the fact that many diverse systems give rise to the same critical exponents, even though their critical temperatures maybe different.

Critical exponents can be defined for the various thermodynamic quantities as shown in the table given below:

Table 1.1: Definition of critical exponents

Quantity	Exponent	Definition
Specific Heat(C)	α	$C = (A/\alpha)t^{-\alpha}$
Order Parameter(M)	β	$M = Bt^{\beta}$
Susceptibility(χ)	γ	$\chi = \Gamma t^{-\gamma}$
Correlation length(<)	ν	$\xi = \xi_p t^{-\nu}$
Critical Isotherm($M(t=0)$)	δ	$M(t=0) \sim H^{\delta}$
Correlation function($G^{(2)}(r)$	η	$G^{(2)}(r) \sim \frac{1}{r^{d-2+\eta}}$

where $t = (T - T_c)/T_c$ for $T > T_c$ and $t = (T_c - T)/T_c$ for $T < T_c$. The exponents are identical for $T < T_c$ and $T > T_c$, but the amplitudes may be different.

The behaviour of the systems may not follow the single exponent behaviour, as defined in the table given above. Due to the presence of some irrelevant variables the critical behaviour is modified to [5]:

$$C_v = At^{-\alpha}[1 + at^{\Delta}] \tag{1.12}$$

Where Δ depends upon the universality class of the system. For example

A ~ 0.55 for the 3d Heisenberg model. An example for an irrelevant variable is the anisotropy in magnetic systems.

1.3 Theoretical models for Ferromagnetic systems

One of the simplest microscopic Hamiltonians to describe magnetic interactions is the Ising model Hamiltonian. The Ising model describes the interactions between spins localized on a lattice. The spins are allowed to be either parallel or anti-parallel to each other. The Hamiltonian for the magnetic interaction is given by

$$H = \sum J_{ij} S_i . S_j \tag{1.13}$$

Where J_{ij} is the strength of the interaction between the spins S_i and S_j . The spins are assumed to be localized at the lattice sites i and j respectively. In the case of the Ising model, the spins at each lattice site can only assume the values -1 or $+1$,i.e, there are only two permitted directions for the spins. This corresponds to the behaviour of a spin $1/2$ particle. If the spins can orient along any direction in a plane, the corresponding model is known as the XY model. If the spin can orient in any direction in **3** dimensions, then it is described by the Heisenberg model.

It is found that the critical behaviour of the ferromagnetic metals like Iron and Nickel are adequately described by the Heisenberg model even though the model assumes the spins to be localized on the lattice sites. As is well known [6], the electrons contributing to the magnetic moment in the case of Nickel are itinerant in character. This is an example of the phenomenon of universality, i.e, the insensitivity of the critical behaviour to the details of the interaction Hamiltonian. The critical exponents seem to depend only on the spatial dimension and the number of components of the order parameter.

The values of the critical exponents and the amplitude ratios A_+/A_- for different space and spin dimensions are given in table 1.1 and table 1.3 respectively. Where A_+ and A_- are the amplitudes for the various thermodynamic quantities above and below T_c.

The tricritical point mentioned in table. 1.2 is the point at which a transition changes over from a first order to a second order transition. In the above table, the exponents for 2d XY and Heisenberg models are not given since it has been proved that a 2 dimensional system having an order parameter with more than one component does not have a transition at a finite temperature [7].

Since the determination of the exponent for specific heat will be dealt with in

Table 1.2: Values of Critical exponents for different universality classes

Model	α	β	γ	ν
2d Ising	0 (log)			
3d Ising	0.11	0.32	1.24	0.63
3d XY	-0.01	0.35	1.32	0.67
3d Heisenbere	-0.12	0.36	1.39	0.71
tricriticalpt	0.5			
Mean Field	0	0.5	1	0.5
Experiment				
3d Ising	0.11	0.32	1.24	0.63
3d Heisenberg	-0.1	0.34	1.4	0.7
2d Ising	0.0	0.3	1.82	1.02

later chapters, a few remarks on the value of this exponent for different models are in order. In the case of the 2d Ising model, the specific heat diverges as

$$C_v = A \log t \tag{1.14}$$

From Fig. 1.2, it is seen that the specific heat rises symmetrically on each side of the critical temperature T_c in the case of the 2-d Ising model. What we see in three dimensions is more characteristic of the real Lambda transition: there is more specific heat on the low-temperature side than on the high temperature side of T_c. This asymmetry seems to be a characteristic change on going from two dimensions to three dimensions [8].

Where t is the reduced temperature given by $t = |(T - T_c)/T_c|$. This result means that the specific heat diverges at the transition temperature. This was predicted by Onsager [9], who gave an analytical solution for the 2-d Ising model. In the case of the 3d Ising model, the specific heat still diverges near the transition point, but with an exponent of 0.11. The specific heat behaviour for the 2d Ising and the 3d Ising models are plotted in Fig. 1.2 for a transition at 300 K. In both cases, the specific heat diverges to infinity. However the specific heat starts diverging farther away from T_c in the case of 2d Ising model than in the case of the 3d Ising model. This indicates that the mean field approximation is valid over a wider range in the case of the 3d Ising model than in the case of the 2d Ising model. This can be understood on the basis of the Ginzburg criterion to be discussed below. In the case of the 3d Heisenberg model, the negative value of a implies that the specific heat increases near T_c, but remains finite at T_c (Fig. 1.3).

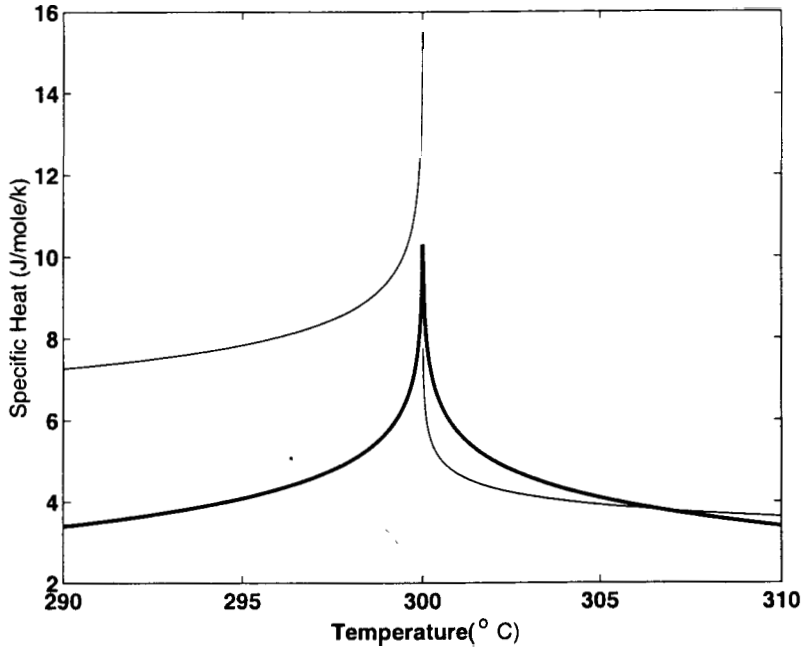

Figure 1.2: Specific heat near T_c for the 2d and the 3d Ising models. Key:- Thin line-3d Ising , Thick line- 2d Ising model

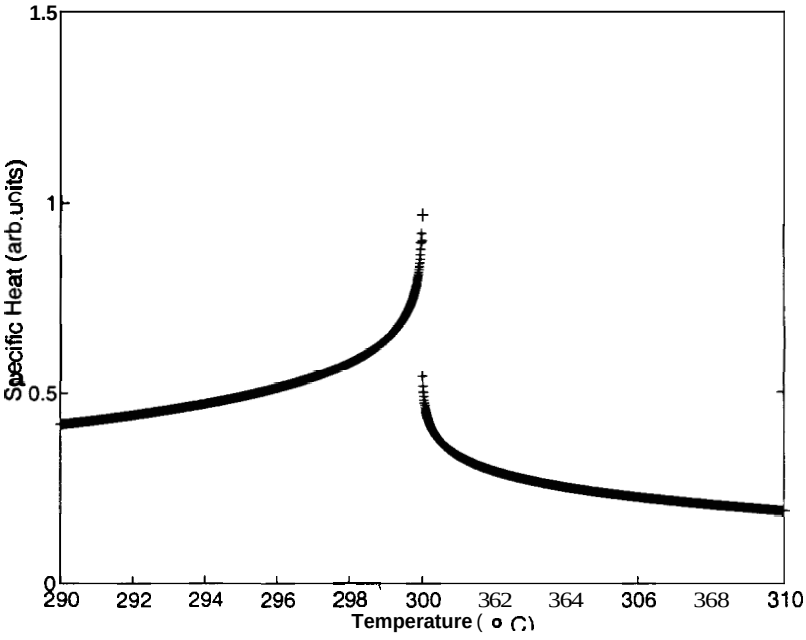

Figure 1.3: The specific heat near T_c for the 3d Heisenberg model

The difference in the behaviour of the Ising and the Heisenberg models can be understood in a qualitative way. In the case of the Ising model, the internal energy changes by $4NJS^2$ for the reversal of each spin [10]. N is the number of spins with which each spin interacts. If 'x' spins reverse direction for unit temperature rise, then the change in the internal energy per unit temperature rise (which is the specific heat) is

$$C_v = 4NxJS^2 \tag{1.15}$$

Now N diverges near T_c, since the correlation length ξ, diverges. N will roughly go as ξ^d (where d is the space dimension). From the above argument it is obvious that the specific heat will diverge in this case because of the divergence in the correlation length.

In the case of the Heisenberg model, the above argument gets slightly modified as the spins can point in any direction, unlike the case of the Ising model where they can only be either parallel or anti-parallel to each other. Therefore Eq. 1.15 is modified to

$$C_v = 4NxJS^2\cos(\theta) \tag{1.16}$$

Where $\cos(\theta)$ is the angle between the interacting spins. As T_c is approached, N goes to infinity, but $\cos(\theta)$ goes to zero (as on the average no two spins will be aligned in the same direction), hence the product of the two can be a finite quantity.

Experimentally, it is very difficult to distinguish between the Ising and Heisenberg models. This is because of the fact that, even though theoretically, the specific heat goes to infinity at T_c in the case of the Ising model, the experimentally measured specific heat remains finite. The experimentally measured specific heat remains finite as we cannot approach arbitrarily close to T_c

The values of the various critical exponents are not all independent since they are related by so-called scaling relations. It turns out that there are only two independent critical exponents. Historically, it was shown by Rushbrooke [11], Griffiths [12], Josephson [13] and Fisher [14]that basic thermodynamics together with a few reasonable assumptions oblige the six exponents to satisfy four inequalities. For example, Rushbrooke derived an inequality connecting $\alpha, \beta and \gamma$ using the fact that the specific heat has to be positive. Similarly another inequality can be derived from the fact that the compressibility is always positive. Gradually, experimental evidence accumulated that these inequalities were in fact equalities and in 1965 Widom [15]

showed two of them would indeed be equalities if the Helmholtz free energy were not any odd function of two variables(eg: temperature and magnetic field), but could be approximated by a function ψ of one variable. For a magnetic system, Widom suggested that near T_c, f (Helmholtz free energy), can be approximated by

$$\mathrm{f}(t,\mathrm{B}) = t^{1/y}\psi(B/t^{x/y}) \tag{1.17}$$

Where t = $\frac{|T-T_c|}{T_c}$.

From this hypothesis we can derive the scaling laws mentioned earlier. They are:

Rushbrooke's law:

$$\alpha + 2\beta + \gamma = 2 \tag{1.18}$$

Griffith's law:

$$\alpha + \beta(\delta + 1) = 2 \tag{1.19}$$

Fisher's Law:

$$(2 - \eta)\nu = \gamma \tag{1.20}$$

Josephson's hyperscaling law:

$$\nu d = 2 - \alpha \tag{1.21}$$

All these laws are valid for all continuous phase transitions and have been experimentally verified. In the case of a mean field transition the hyperscaling law is valid only for one particular dimension known as the 'upper critical dimension'. This is so since the mean field exponents are independent of the spatial dimension. The concept of 'Upper critical dimension' will be introduced in the next section.

The values of experimentally determined critical exponents could be useful to assign a given system to a particular universality class (Model). However as is noticeable from the table, the values of critical exponents for different universality classes are quite close to each other. Hence a better way to study critical phenomena would be to determine the amplitude ratios, which are listed below for various systems.

Table 1.3: Values of amplitude ratios

3d Theory	A_+/A_-	ILK-	ξ_+/ξ'_-
Ising	0.52	4.9	1.9
XY	1.0		0.33
Heisenberg	1.52		0.38
3d Experiment			
Ising	0.5 - 0.63	4.5 - 5.0	2.0
XY	0.49 - 0.74	5.0	1.7 - 2.0
Heisenberg	0.84 - 1.6		1.8

Mean field theories are valid for d > 4. This can be proved using a simple criterion given by Ginzburg [3].

Basically the criterion says that mean field theories are valid if the square of the fluctuations is much less than the square of the order parameter. As can be seen intuitively , the effect of fluctuations is less in higher dimensions. This is because each spin has more number of neighbours in higher dimensions and therefore the energy required to cause a fluctuation is much greater in higher dimensions (crudely speaking, more bonds have to be broken in higher dimensions). For d < 4 , the Ginzburg criterion gives the range of temperature from T_c beyond which mean field theory is valid. The dimension above which mean field theory is valid is known as the upper critical dimension. The upper critical dimension depends on the Hamiltonian chosen to describe the system. For example if the Hamiltonian has only the M^6 and M^2 terms, the upper critical dimension is **3.** Hence mean field theories are quite suitable for a system described by such a Hamiltonian in **3** dimensions.

For d < d_c, where d_c is the upper critical dimension, mean field theory is valid for temperatures sufficiently far from T_c. As T approaches T_c (either from above or from below), fluctuations become more important and the inequality is violated. The temperature T_G at which fluctuations become important is called the Ginzburg temperature and is given by

$$t_G = \frac{|T_G - T_c|}{T_c} = \left(\frac{A_d}{2\Delta C_v \xi_o^d}\right)^{\frac{2}{7}4-d} \tag{1.22}$$

Where A_d is a constant for a fixed dimension d. $\xi_o = \left(\frac{c}{aT_c}\right)^{1/2}$ is the bare coherence length and $\Delta C_v = \frac{a_o^2 T_c}{8b}$ is the mean-field specific heat jump per unit volume.

Thus, mean field theory will be valid even very close to a critical point for

d < d_c, if the bare coherence length ξ_o is large. This is the case for systems with long range forces. When $|T_G - T_c|$ is not small, one can expect a crossover from mean field behaviour to critical behaviour when the reduced temperature t = $\frac{T-T_c}{T_c}$ becomes of order t_G.

In 3-d, a careful evaluation of A_d yields [3]

$$t_G = \frac{k_B^2}{32\pi^2(\Delta C_v)^2\xi_o^6} \tag{1.23}$$

1.4 Phase Transitions under High Pressure

In most of the discussion about phase transitions given above, temperature seems to play the predominant role as far as the free energy of the system is concerned. However the free energy of the system is also dependent on the pressure to which the system is subjected to. The application of pressure changes the interatomic interactions, leading to the appearance of new phases. In some cases, phases which are not seen at atmospheric pressures, make their appearance at higher pressures. There have been a few instances of re-entrant phase transitions at high pressures. This phenomenon has been observed in the case of metallic glasses and also in the case of liquids [16] and liquid crystals.

Since the later chapters will deal with phase diagrams quite extensively, a general introduction to the concepts involved, is given in this section. Fig. 1.4 shows a general phase diagram for a material, showing the three states of matter -solid, liquid and gas. In the solid state some materials have a ferromagnetic phase, which is demarcated from the paramagnetic phase by the dashed line in Fig. 1.4. The ferromagnetic phase has a spontaneous magnetization, which is destroyed by an increase in temperature. With a further increase in temperature, the positional order which is characteristic of the solids is destroyed when there is a transition to the liquid state. In the case of some organic systems, there is an intermediate state between the solid and the liquid phases, where the orientational order of the molecules is retained, but the positional order maybe partially (in some directions) destroyed. This phase is known as the liquid-crystalline phase, since it has properties of both the liquid and the crystalline phases. The liquid state transforms to the gaseous phase when the temperature is increased beyond the boiling point.

The liquid-gas phase boundary terminates at a critical point (T_c, P_c) beyond which there is no distinction between the liquid and the gas. At temperatures and pressures greater than the T_c and P_c, the liquid can transform continuously into the

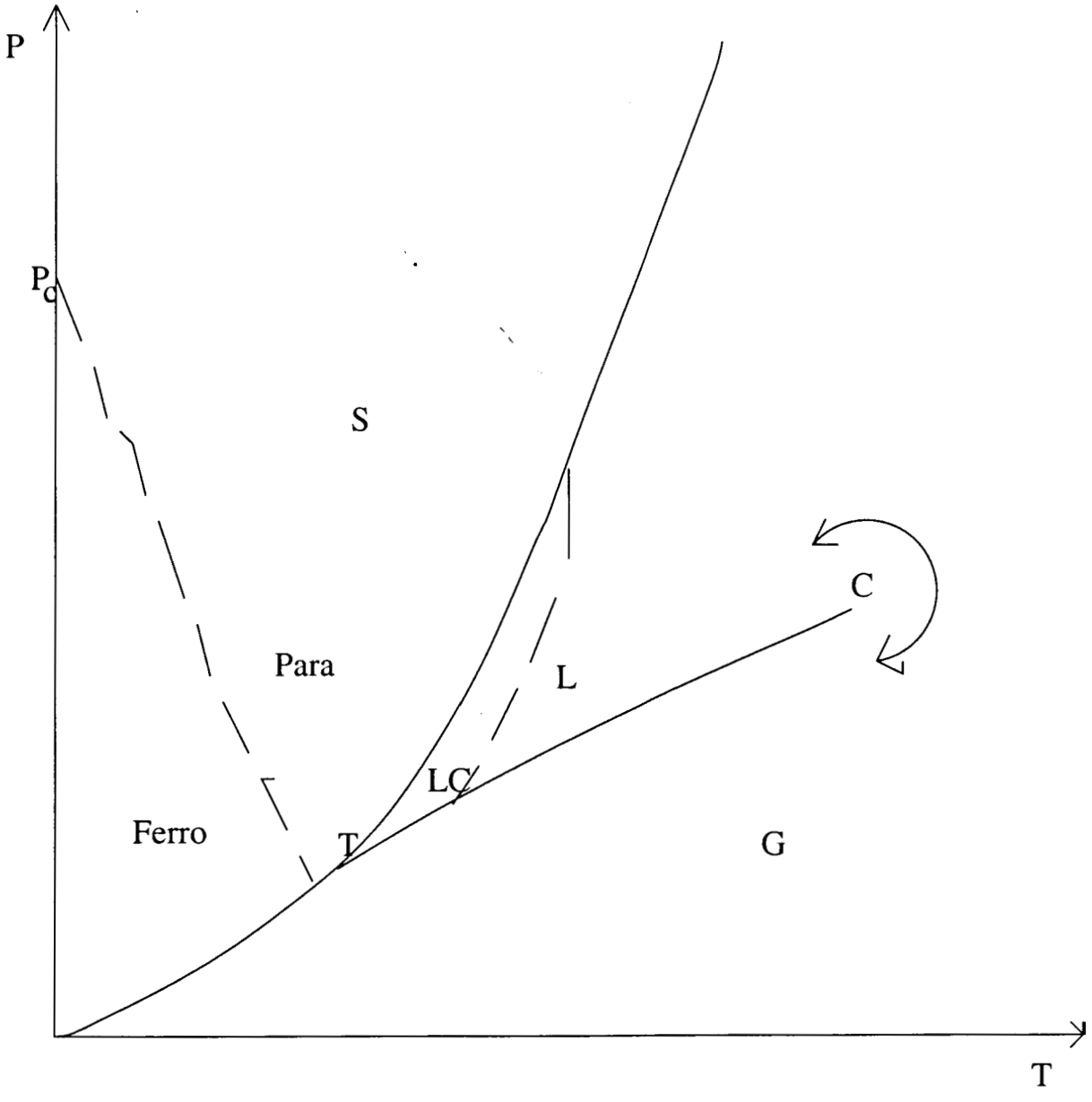

Figure 1.4: A typical Phase diagram showing the various possible phases

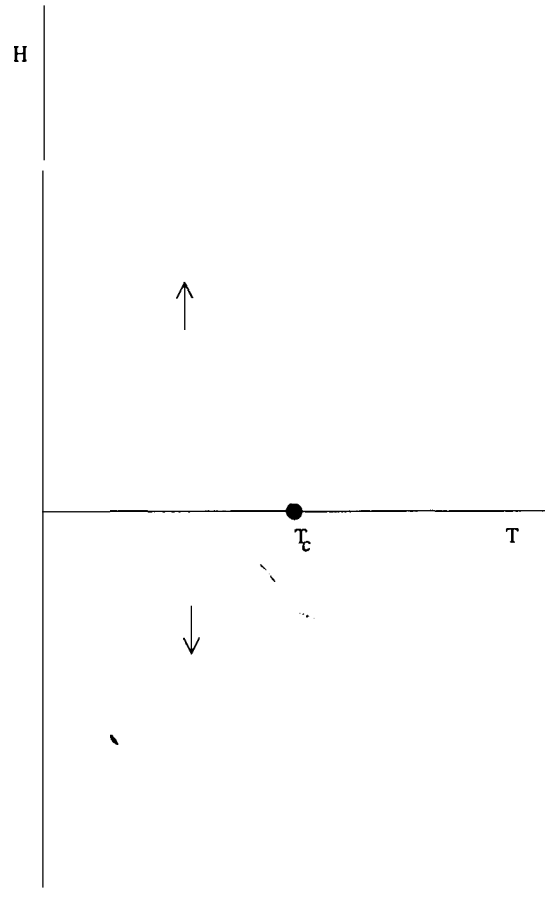

Figure 1.5: Phase diagram for a ferromagnetic system showing the critical point

gaseous phase. This is possible as there is no symmetry difference between the liquid and the gaseous phase. Both the solid-liquid transition and the liquid-gas transition (except at the critical point), are first order transitions.

The phase boundaries (in the case of first order transitions) are described by the Clausius-Clayperon relation [2]:

$$\frac{dP}{dT} = \frac{\Delta S}{\Delta V} \tag{1.24}$$

A positive slope for the phase boundary means that both ΔS and ΔV are positive or both of them are negative (which is more unlikely). A negative slope usually implies that ΔV is negative . The only example for a negative ΔS is the liquid-solid transition in Helium where the liquid phase is more ordered [2]. ΔV is negative in the case of the melting transition in water.

The liquid-gas transition has many analogies with the ferromagnetic to para-

magnetic transition. In the case of the ferro-para transition, the magnetization is analogous to volume, while the magnetic field is analogous to the pressure. The phase diagram for the ferro-para transition is shown in Fig. 1.5. The critical behaviour around this critical point fits the 3d Ising model.

In the case of a continuous phase transition, the R.H.S of Eq. 1.24 becomes indeterminate as both A S and ΔV become zero for a continuous transition. In that case the R.H.S of Eq. 1.24 is evaluated'using L'Hospital's rule. Differentiating the numerator and the denominator of the indeterminate expression with respect to T, we have,

$$\frac{dP}{dT} = \frac{\Delta C_v}{VT\Delta\alpha} \tag{1.25}$$

Where ΔC_v is the discontinuity in specific heat and An, the discontinuity in the coefficient of volume expansion.

Differentiating Eq. 1.24 with respect to P one obtains the other Ehrenfest relation for a second-order transition [2]:

$$\frac{dP}{dT} = \frac{\Delta\alpha}{\Delta\beta} \tag{1.26}$$

Where $\Delta\beta$ is the discontinuity in compressibility at the transition.

High pressure studies are also undertaken to investigate various multicritical points [17] which occur in some systems.

1.5 Amorphous Magnetic systems

While critical phenomena in crystalline magnetic systems have been receiving quite a bit of attention over a very long time, the critical behaviour of amorphous magnetic systems has been studied only quite recently. The number of experimental studies have been somewhat limited. The present study on amorphous magnetic systems was motivated by a number of fundamental questions regarding the behaviour of amorphous systems:

What is the nature of the critical behaviour in amorphous magnetic systems? Is there a marked departure with respect to the corresponding crystalline systems?

Gubanov [18] showed that Ferromagnetism could exist in the amorphous state. Harris [19] gave a physical estimate of the effect of fluctuations in T_c due to the presence of non-magnetic components in the sample as well as the fluctuations in J_{ij} due to variations in the nearest neighbour distance.

The argument of Harris is as follows:

Divide the magnetic system into cells of dimension L. L is chosen to be of the order of the correlation length ξ, so that the cells are sufficiently large to have a well defined average concentration of impurities but are weakly correlated. Let T_c be the average transition temperature and the fluctuations in T_c are estimated from cell to cell.

From central limit theorem, we expect that

$$\Delta T_c \sim (n)^{-1/2} \sim L^{-d/2} \tag{1.27}$$

where n is the number of impurities in each cell.

Rewriting the above equation, we have,

$$\Delta T_c \sim \xi^{-d/2} \sim |T_c - T|^{d\nu/2} \tag{1.28}$$

As long as AT, $< |T_c - T|$, the fluctuations in T_c will not round the transition and this requires that $d\nu/2 > 1$ or using the scaling relation $d\nu = 2 - \mathrm{a}$, we find $\mathrm{a} < 0$ as the condition for a sharp T_c. Only the *3d* Ising model is thought to have $\mathrm{a} < 0$. Luther and Grinstein [20] and Lubensky [21] have studied magnetic systems near $d = 4$ with small fluctuations in the exchange parameters using the renormalization group and concluded that when the Harris criterion is satisfied, the fluctuations due to a small amount of randomness are irrelevant. For $\mathrm{a} > 0$, they found a new fixed point with different critical exponents.

According to this argument, the systems obeying the Heisenberg model should not be affected by positional disorder as $\mathrm{a} < 0$ for these systems. The Harris criterion only says whether the transition will be sharp or not i.e, whether the system has a single transition temperature or the transition occurs over a range of temperatures. It does not tell anything about the nature of the critical behaviour. Grinstein and Luther [20] proved that the critical exponents also do not change if the Harris criterion is satisfied. However they proved this result for the case of weak disorder. The theoretical situation has not been clarified for the case of strong disorder as in the case of metallic glasses.

There are only a few experimental results [22] to show that disorder has no discerneble effect on the critical exponents.

References

[1] H.E.Stanley, *Introduction* to Phase transitions and Critical Phenomena, Oxford University Press, 1971

[2] A.B.Pippard, Classical Thermodynamics, Cambridge University Press, 1963

[3] P.M. Chaikin and T.C. Lubensky, Principles of Condensed Matter Physics, Cambridge University Press, 1995

[4] K.G.Wilson, Phys.Rep, **12c**, 76 (1974)

[5] Wegner F.J., Phys.Rev.B., 5, 1889 (1972)

[6] E.Fawcett and W.A.Reed, Phys.Rev.Lett., 9, 336 (1962); E.Fawcett, Adv.Phys., 13, 139 (1964); A.S.Joseph and A.C.Thorsen, Phys.Rev.Lett., 11, 554 (1963); D.C.Tsui and R.W.Stark, Phy.Rev.Lett., 17, 871 (1966); L.Hodges,D.R.Stone and A.V.Gold, Phys.Rev.Lett., 19, 655 (1967)

[7] N.D.Mermin and D.Wagner,Phys.Rev.Lett., **17,** 1133 (1966)

[8] M.E.Fisher, Essays in Physics, vol.4, Ed.G.K.T.Conn and G.N.Fowler, Academic Press, 1972

[9] L.Onsager, Phys.Rev., **65**, 117 (1944)

[10] C.Kittel, Introduction to Solid State Physics, Wiley Eastern Pvt. ltd., New Delhi, 1971

[11] Rushbrooke, J.Chem¿Phys., 39, 842 (1963)

[12] R.B.Griffiths, Phys.Rev.Lett., **14**, 623 (1965)

[13] B.D.Josephson, Proc.Phys.Soc., **92**, 269 (1967)

[14] M.E.Fisher, Phys.Rev., **180**, 594 (1969)

[15] B.Widom, J.Chem.Phys., 43, 3892 (1965)

[16] Anil Kumar and T.Narayanan, Phys.Rep.,249, 135 (1994)

[17] Anil Kumar, H.R.Krishnamurthy and E.S.R.Gopal, Phys.Rep., 98, 57 (1983)

[18] A.I.Gubanov in Quantum Electron Theory of Amorphous Conductors, Consultants Bureau, New York, 1965

[19] A.B. Harris, J.Phys.C**7**, 1671 (1974)

[20] A.Grinstein and A.Luther, Phys.Rev.B **13,** 1329 (1976)

[21] T.C.Lubensky in Ill-Condensed Matter, Proceedings of Les Houches school, Edited by Roger Balian, Roger Maynard and Gerard Toulouse, 1978

[22] L.J. Schowalter, M.B. Salamon, C.C.Tsuei and R.A. Craven, Sol.State.Comm, 24, 525 (1977)

Chapter 2

High Pressure Instrumentation

2.1 Introduction

The Piston-cylinder apparatus is a well known device in the field of high pressure research. The piston-cylinder device used in the present work can attain pressures of the order of 50 kbars. The maximum pressure which can be attained is set by the strength of the tungsten carbide plates which are used to contain the sample. While higher pressures are obtained in the Diamond anvil technique, the piston-cylinder technique has the advantages of a large sample size and a true hydrostatic pressure.

The piston-cylinder apparatus is discussed in detail in this chapter. The cell-assemblies used in the present experimental work, as well as the techniques used for the measurement of resistivity and thermopower are also described.

2.2 Piston-Cylinder Apparatus

The high pressure apparatus used in the present investigation is a piston-cylinder device and very high pressures can be generated by the advance of a one inch or half inch diameter piston into a cylinder, both made of tungsten carbide (WC). The entire arrangement (Fig. 2.1) consists of a ten inch diameter master ram of 1000 ton capacity. The entire arrangment of the pistion-cylinder apparatus together with the pressure controls is shown in the photograph appearing in the next page. The piston assembly is advanced by operating this master ram. Since WC is strong in compression and weak in tension or shear, precautions have to be taken to see that it is always under compressive load. When high pressure is generated in the cylindrical WC core there will be a tensile lateral force acting along the axis of the cylinder. To compensate for this, the cylinder is supported axially by an end load ram of 750 ton capacity. The pressure plate assembly and the end load plate are

shown in Fig. 2.2 and Fig. 2.3, respectively. The WC core (with a cylindrical hole) is fitted into binding rings of hardened EN24 steel. The purpose of the binding rings and the end load is to provide support for the WC core. If the core is not inside the binding ring when high pressure is generated inside the cylinder , compressive radial stresses and tensile hoop stresses will be created. This causes a shear along which the carbide may fail. Since the binding rings are interference fitted to the WC core, both these stresses become compressive so that the shear in the X-Y plane perpendicular to the ram movement along Z is minimized. However, if there is no stress along Z axis, there would be no shear in the vertical plane, which the end load ram counteracts. This arrangement vastly enhances the normal operational capability of an unsupported WC core. The minimization of the unsupported part of the piston is a major requirement to attain pressures of the order of 50 kbars.

2.3 High Pressure Cells

2.3.1 Teflon cell technique for measurement of Resistivity and Thermopower of Metals

The advantage of this technique is that measurements of these properties can be made under truly hydrostatic pressures of the order of 50 kbar [1]. We have used a teflon cell container described by Jayaraman et al [2] for generating high pressure *in situ* over the sample. To create a steady temperature difference between the ends of the sample, which is essential for TEP measurements it is necessary to partition the Teflon container in such a way that the convection mixing of the Silicon oil used as pressure transmitting medium, is minimized. This has been achieved by piercing the sample through the teflon disc (3mm thick and 19 mm diameter) as shown in Fig. 2.4. The disc when inserted into the Teflon container, effectively partitions the pressure transmitting medium and helps maintain a steady temperature difference. The Silicone oil on either side of the disc is heated to different temperatures using two Nichrome heaters of different resistances threaded through mica discs. They are either connected in parallel or can be taken out separately through the teflon cap. Two pairs of Chrome1 and Alumel thermocouple wires are spot-welded to either end of the sample and brought out through the cap of the teflon cell container as shown in Fig. 2.4 The specimen holder is machined from a solid teflon rod so that the disc and the cylindrical projection on either side form an integral part. The thermocouple wires are inserted through the pyrophyllite plug and brought out through the cap of the teflon container. The thermocouple probes and heater leads are taken out from

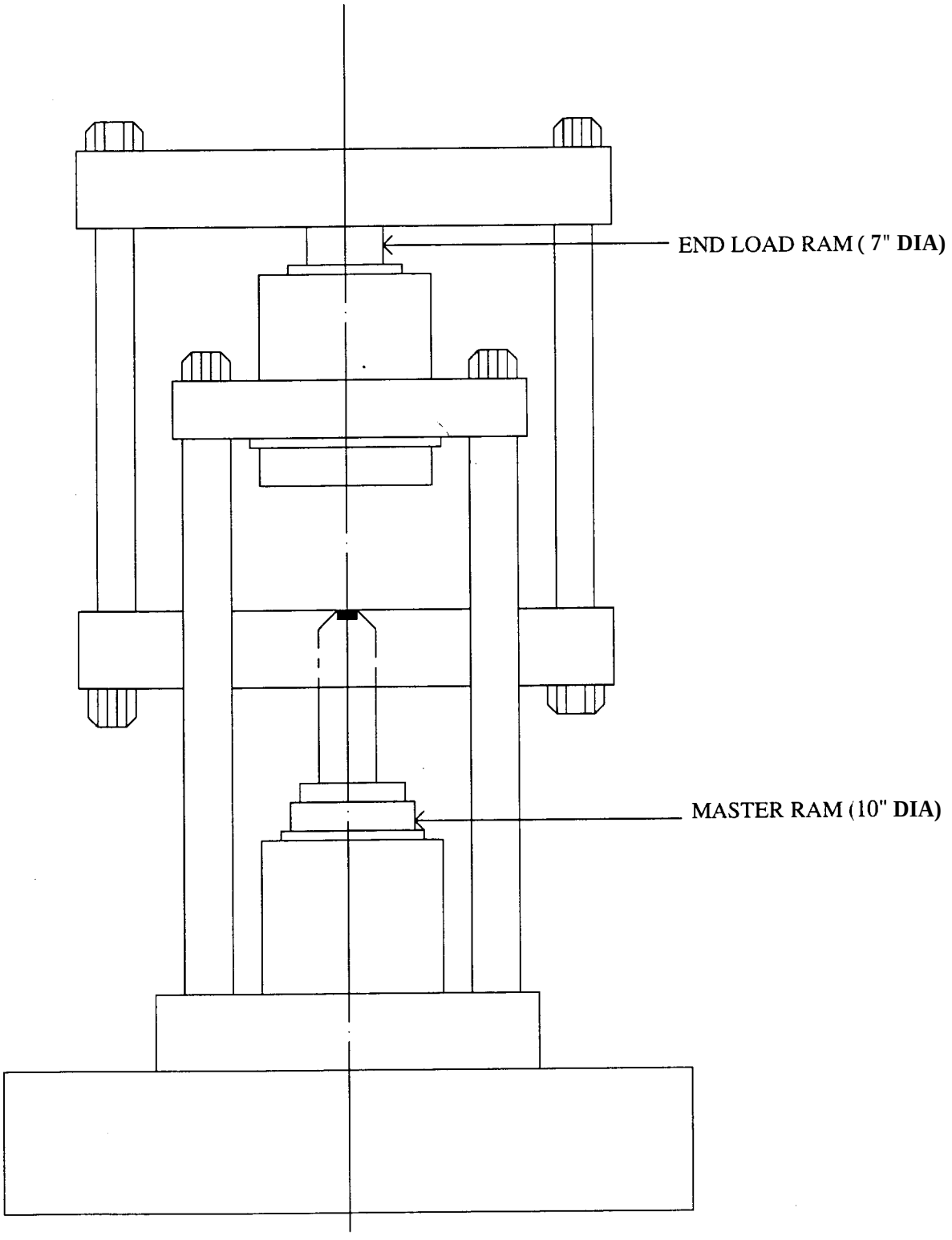

Figure 2.1: Piston-Cylinder device

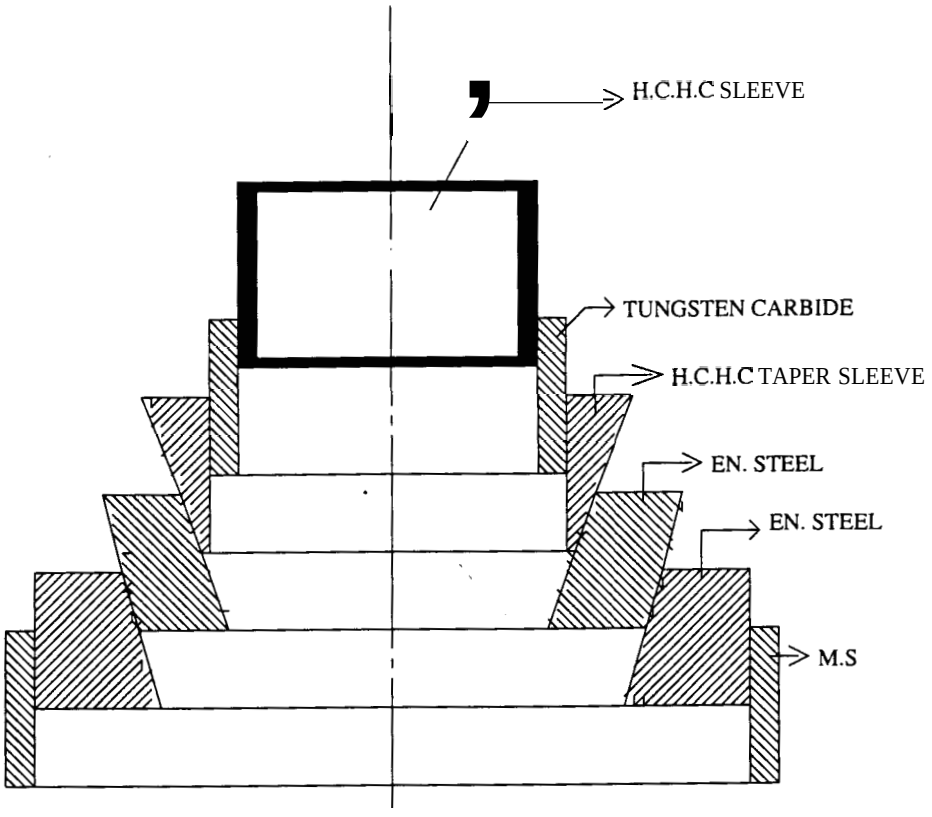

Figure 2.2: Pressure Plate Assembly

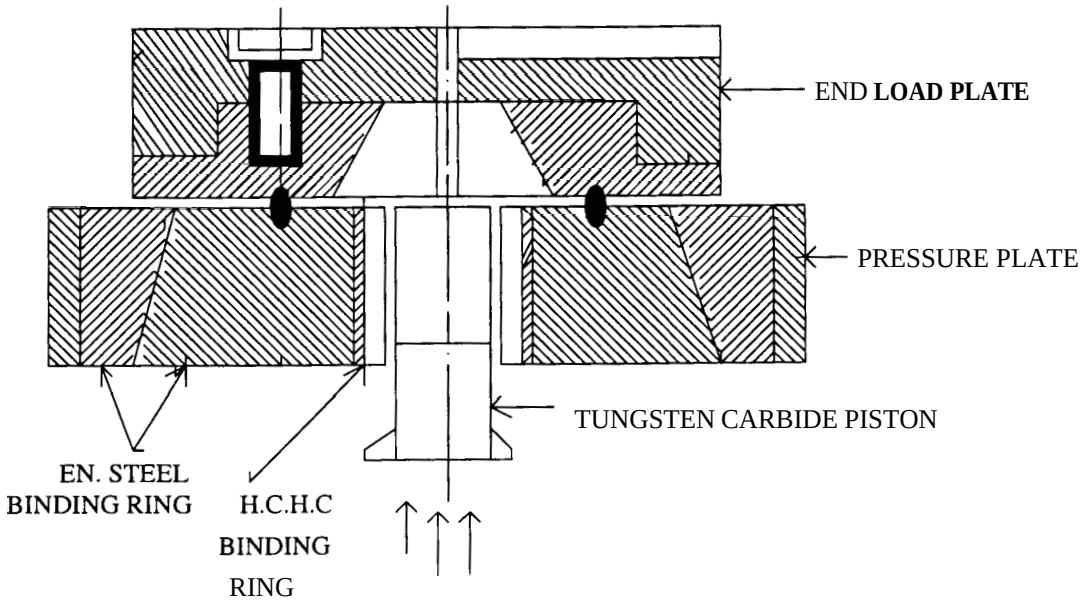

Figure **2.3:** Pressure Plate With End load Plate

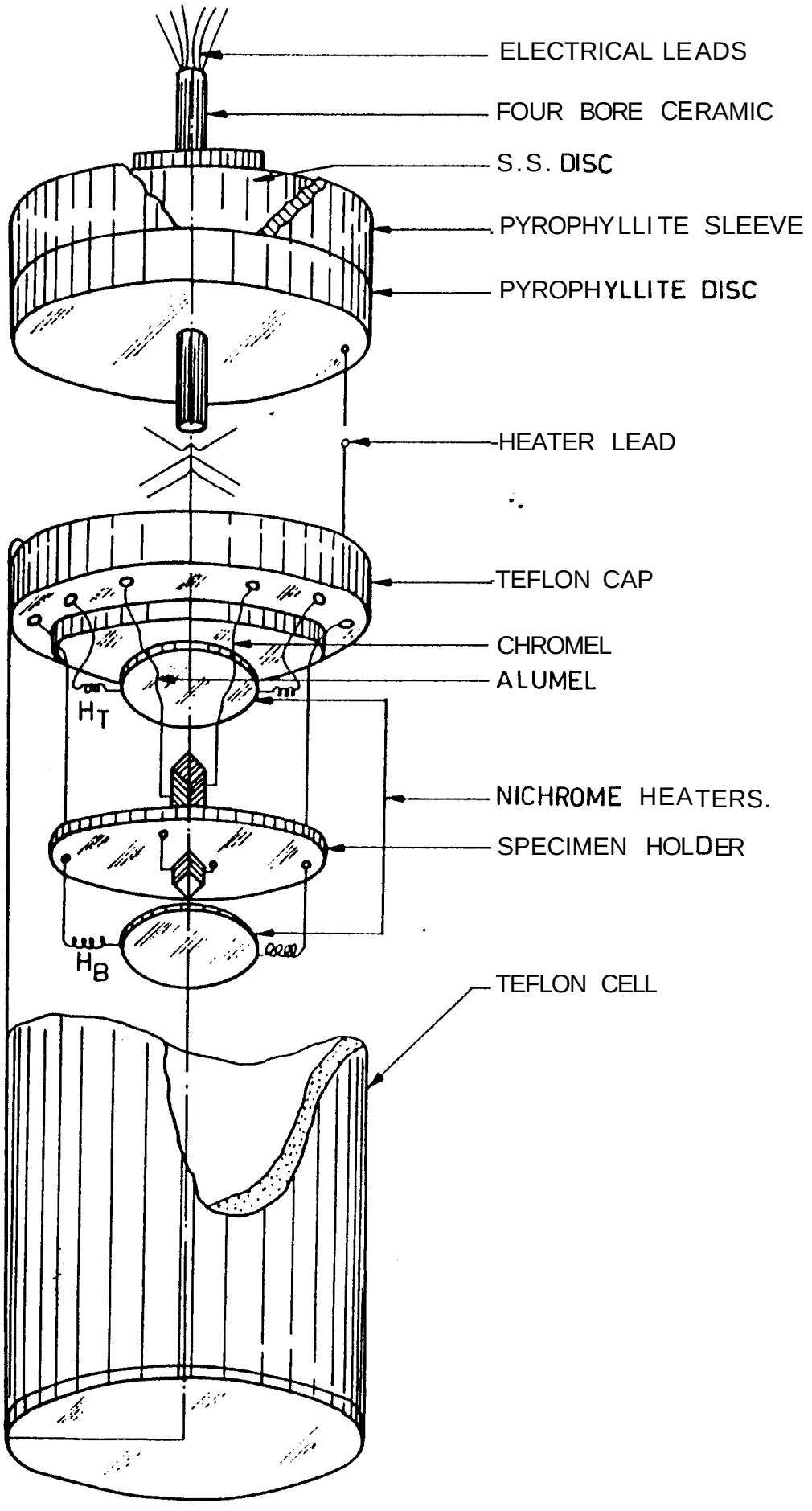

Fig. 2.4 Schematic diagram of the Teflon cell

the high pressure region to the atmospheric pressure region in a manner described by Jayaraman et al [2]. The thermocouple leads are taken out through four hole ceramic tubings and connected to the appropriate wires coming out of the cap of the teflon cell by spot-welding the junction. By this the generation of thermo-electric noise voltages due to temperature fluctuations is completely avoided as no new metal is used for bonding. The pyrophyllite disc and the stainless steel piece with a pyrophyllite ring assembly, through which the ceramic tubing is inserted helps in holding the ceramic tube in position under pressure. At low pressures the stainless steel disc flows and grips the ceramic whereas at high pressures the lower pyrophyllite disc provides the necessary grip for the ceramic. One of the heater leads which passes through the hole in the pyrophyllite disc makes contact with the stainless steel piece which in turn will be touching the end load plate of the pressure chamber. The other heater wire touches the pressure plate directly. The pressure plate and the end load plate which are insulated from each other acts as the terminals for current to be passed. The teflon cell assembly is positioned inside the pressure chamber. The pressure chamber made out of the WC core fitted with steel binding rings described earlier is the one used in the piston-cylinder device.

In any pressure experiment, there will always be a small length of the wire that suffers a large pressure gradient while it is brought from the high pressure to the atmospheric pressure region. This small region is inhomogeneous in its properties and for TEP measurements it is essential that in these portions of the wire there are no temperature gradients. The cell we are using almost satisfies this requirement because of the internal heating arrangement and smaller diameter of wires used which reduces thermal conduction through the wires. The cell provides a temperature gradient varying from 0.25" C to 15° C in the temperature range 0-250° C.

The same cell can also be used for 4-probe resistivity measurement. The only modification required would be to see that no temperature gradient exists across the sample. This is achieved by positioning the sample horizontally in the cell and removing the partitioning disc.

The teflon cell has been used for measuring the resistivity and thermopower of Chromium alloys. These are dealt with in chapter 6.

2.3.2 High Temperature High Pressure Cell

The teflon cell technique has a major limitation in that the temperature of the investigation is limited to around 250° C. The development of a talc-graphite-boron nitride assembly **[3]** permits measurement of absolute TEP and resistivity of solids

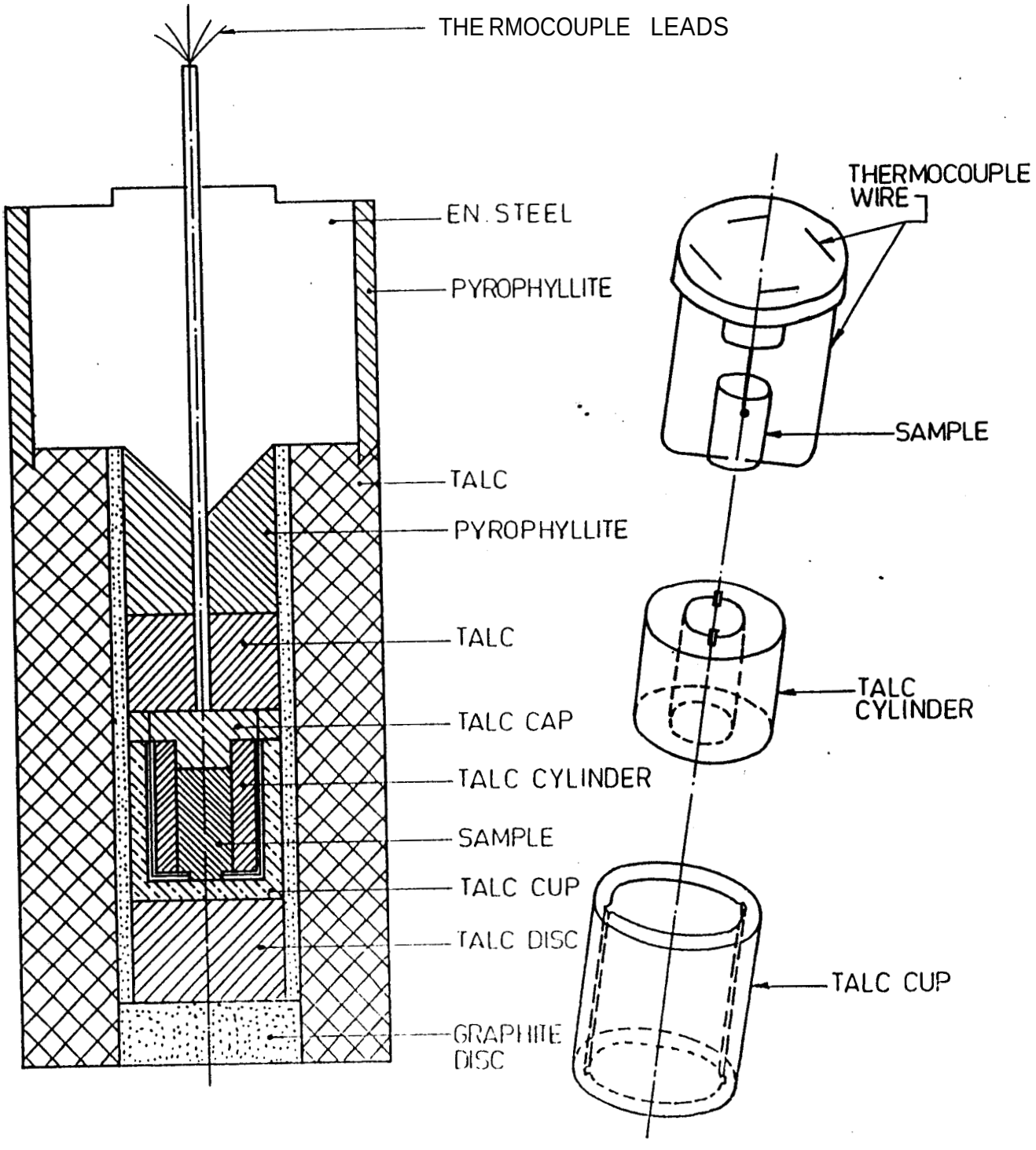

Fig.2.5 The High Temperature-High Pressure Cell

and liquids in the temperature range 0 - 1000" C and 50 kbar pressure. The temperature profile in a graphite heater will in general have a non-uniform temperature zone near the ends and a constant temperature zone in the region away from the ends of the heater. The constant temperature zone is normally located in the vicinity of the geometric center of the furnace and is usually of one quarter of the length in its spread. Since for the measurement of TEP the specimen has to be subjected to a temperature gradient, the natural temperature profile of the furnace can be exploited by proper positioning of the specimen in the furnace.

Talc and pyrophyllite are good solid pressure transmitters and can also stand high temperatures which has made them suitable for our use. These materials, unlike the fluid (Silicone oil) used in the teflon cell technique, cannot produce a truly hydrostatic pressure over the sample. Although the distribution of pressure is not uniform over a wide region, by using small samples (0.5 x 0.5 x 0.2 mm^3) it is possible to subject it to nearly hydrostatic pressure conditions.

The thermocouple leads are either spot-welded or embedded in to the specimen and are taken out through the side holes in the sleeve along the grooves made on its surface which are 90" apart. The sleeve-specimen assembly is inserted into a Boron Nitride cup and the four leads were threaded through the boron nitride cap. These four leads are brought out from the high pressure to the atmospheric pressure region in a way similar to that in teflon cell technique. As boron nitride which is a good thermal conductor is used to contain the sample, the temperature gradients in the regions where the leads suffer a large pressure gradient is minimized.

The graphite heater is powered from a high current (500 Amps) low voltage (10 V) transformer. The current through the heater can be increased gradually by a continuous scan of the voltage on the primary side of the transformer with the help of a motor-gear arrangement coupled to the transformer. This facility allows one to select a convenient heating rate.

The cell for resistivity measurement is the same as above except for the positioning of the sample. For resistivity measurements the important requirement is that the temperature gradient across the sample length should be minimized. This is achieved by keeping the sample horizontally inside the boron nitride container which is a good thermal conductor and also by placing the sample in the constant temperature zone of the graphite furnace. The effects of non-hydrostatic pressure distribution can be further minimized if the distance between the two voltage leads in the four probe method of measuring the resistivity is made smaller. Then one would be measuring that part of the resistance between these two voltage leads

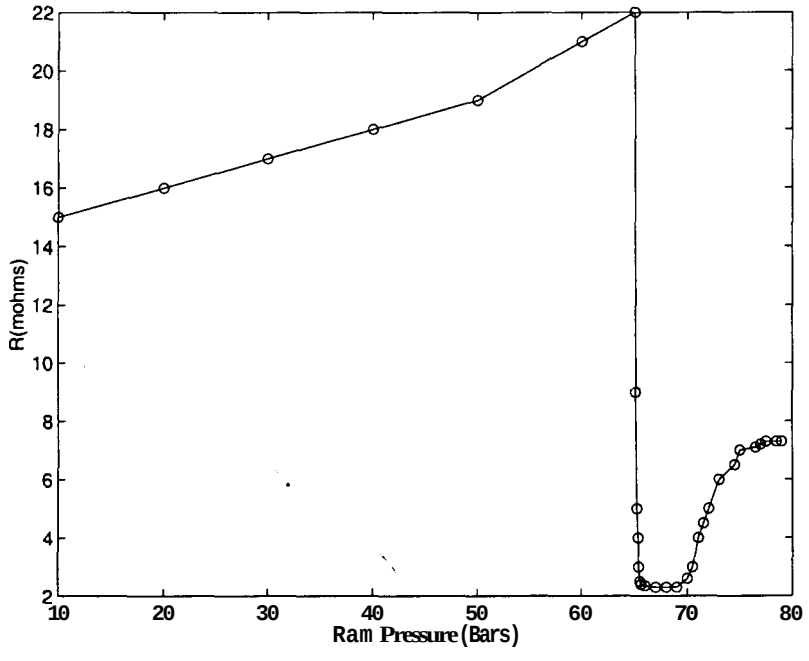

Figure 2.6: Resistance versus Pressure for Bismuth in a 1/2" Teflon cell

which is subjected to nearly hydrostatic pressure conditions, although the rest of the sample is in the non uniform pressure region.

2.3.3 Pressure Calibration

There has been an extensive survey on the problem of high pressure calibration in different pressure and temperature ranges [4]. This problem will not be dwelt with in detail except to give the pressure calibration procedures which were carried out for the present system [5], using the high pressure cells described in the previous sections.

The pressure calibration at room temperature was done by the standard fixed point method resulting from polymorphic phase transitions in some well known metals. In the pressure range 0-40 kbar, the Bismuth I-II and II-III transitions were utilized to calibrate the ram pressure against the true pressure seen by the specimen in different cells. Electrical resistance measurements were done to monitor these phase transitions. Fig. 2.6 and Fig. 2.7 give the relative resistance versus pressure graph for high purity (99.99%) bismuth at 25^o C in the 1/2" teflon cell and 1/2" high temperature high pressure cell. Similar runs were carried out in the 1" teflon and 1" high temperature high pressure cells. Table. 2.1 summarizes the pressure

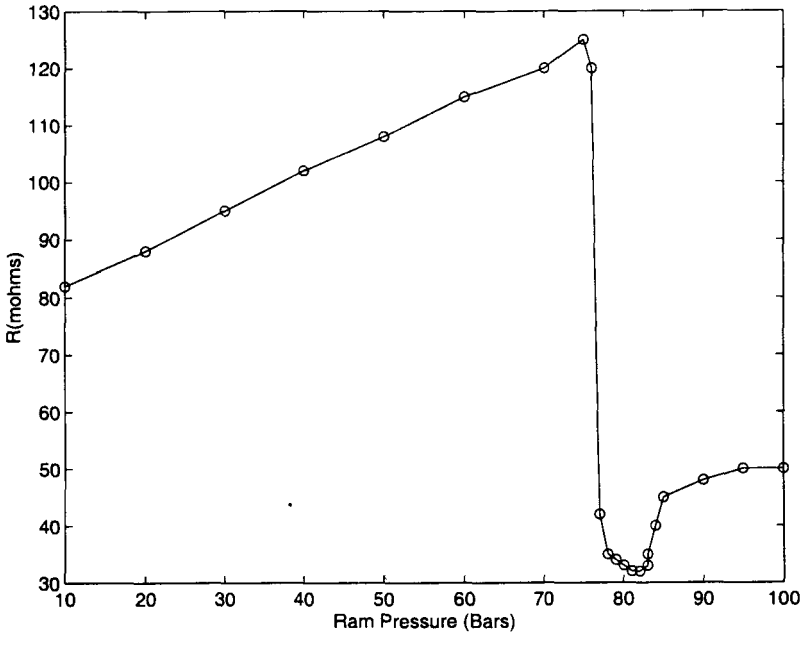

Figure 2.7: Resistance versus Pressure for Bismuth in a 1/2" High temperature cell

calibration data. It is clear from Fig. 2.6 that the bismuth transition in the solid pressure transmitting medium is as sharp as in the truly hydrostatic medium (1/2" teflon cell). This provides direct evidence for the contention that close to hydrostatic conditions can be achieved by making the distance between voltage leads smaller. The resistance variation of manganin wire with pressure was also measured up to **30** kbars Using the established pressure coefficient of resistance for manganin, the ram pressures can be calibrated. This agrees very well with the pressures calculated using the 'fixed' point data.

The problem of pressure calibration at high temperatures is fraught with serious problems. High temperature affects the pressure in a number of ways. **1)** It tends to increase the pressure due to the restraint of thermal expansion of the heated parts of the cell by the surrounding cooler parts of the cell and the pressure cell. 2) It tends to decrease pressure when it causes phase transformation to more dense structures to occur in the sample holder or its contents, and **3)** it may decrease pressure by accelerating the relaxation of the tension in the high pressure chamber. It is pretty difficult to estimate the net effect of these pressure modifying factors and further even temperature measurements at high pressures is not too straight forward in view of the modified calibration characteristics. Strong and Bundy [6] have considered this problem in depth and shown that Iron and Gold can be used as

pressure calibrants at high temperatures. The $a-\gamma$ (BCC $\rightarrow$ FCC) phase boundary in Iron has a good pressure sensitivity of about -4^o C/kbar in the pressure region 20-60 kbar. Further this transformation can be easily monitored by either electrical resistance or TEP measurements. Since the $a-$ y boundary has been accurately established due to the painstaking efforts of several workers in this field, pressure calibration up to 800^o C can be easily carried out. Table. 2.2 summarizes .the calibration data for our high pressure , obtained through a number of experiments on the $a-\gamma$ transition in Iron using both resistivity and TEP as tools. Chromel-Alumel thermocouple which has a small pressure calibration error [7] was used for temperature measurement in this work.

Table 2.1:

Description of the cell	Scale Factor to convert line pressure to true pressure
1" Teflon cell	0.914
1" High temperature cell	0.796
1/2" Teflon cell	0.937
1/2" High temperature cell	0.817

Table 2.2:

Temperature of transition	True pressure of transition	Observed pressure	Sale factor
690^o C	26.8 kbar	34 kbar	1.26
720^o C	25.6 kbar	28 kbar	1.10

2.4 AC Resistivity Technique

The AC resistivity technique used here has been described earlier in the literature. Only a brief description will be given below.

Four leads are spot-welded at the ends of the sample, which is in the form of a thin foil, 20-40 microns in thickness. Two for passing a sinusoidal current through the sample and the other two for measuring the resultant voltage across the sample. Usually two more leads are required to measure the sample temperature. However a novel technique developed by V.Shubha and T.G.Ramesh [8] enables the sample temperature to be measured from these four leads only, without the necessity for

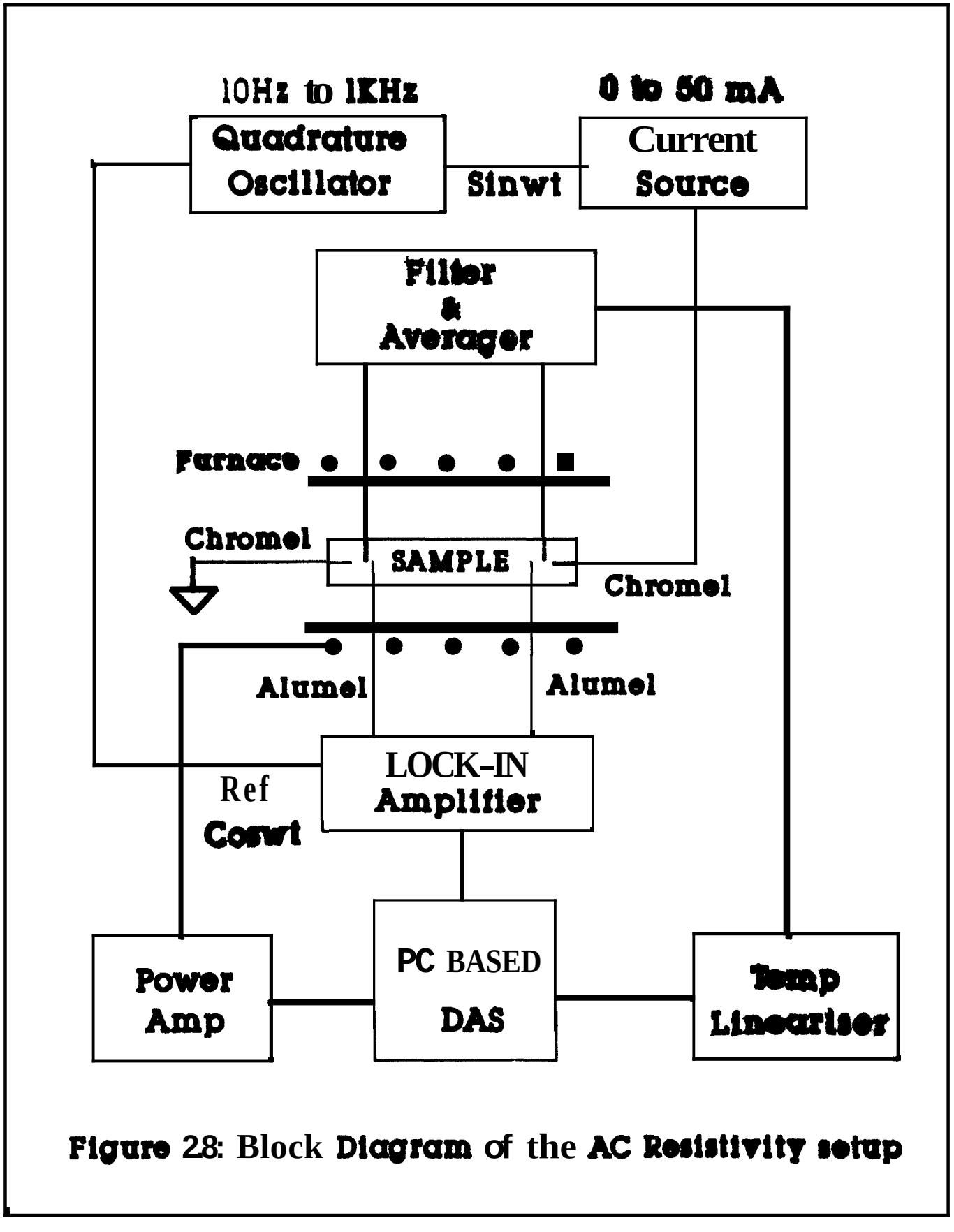

Figure 28: Block Diagram of the AC Resistivity setup

two extra leads. The standard technique which requires six leads to be taken out from the high pressure cell of diameter less than 12 mm is quite difficult.

The two wires attached at each end of the sample are actually Chromel-Alumel thermocouple wires. The AC current is passed through Chrome1 wires, while the voltage across the sample is measured using the Alumel wires.

Fig. 2.8 gives the block diagram of the AC resistivity set-up. The system consists of a quadrature oscillator, a high output impedance AC constant current source and a lock-in amplifier coupled to a PC using the IEEE 488.2 interface. The quadrature oscillator constructed out of two analog multipliers features two sine wave outputs at quadrature whose frequency can be varied from 10 Hz to 1 kHz. One of the sine wave outputs forms the reference signal for the lock-in amplifier. while the other output drives a constant current source. The design of the constant current source is centered around the well known Howland circuit. It would suffice here to mention that the current could be varied continuously from 0-50 mA and the high output impedance ($\sim$ several megaohms) ensures that the current through the metallic sample is constant($\sim$ 0.01%) irrespective of its impedance. The AC voltage developed across the sample which is proportional to the sample resistance is measured with a lock-in amplifier. The frequency of the AC signal is chosen to be around 400 Hz to minimize line frequency noise. The output voltage from the lock-in amplifier is accessed in the PC.

Simultaneous measurement of temperature is achieved by measuring the DC component of the differential voltage developed across the current and voltage leads which are in close proximity. The contribution to the DC voltage from the small portion of the sample between these two leads is negligible by the law of intermediate metals. **A** low pass active filter removes the AC component and the DC output forms the input to a temperature linearizer. In this setup it is possible to detect changes of resistivity of the order of 1 part in a 1000.

2.5 TEP measuring system

For measuring the TEP , the sample is placed along the axis of the cell described earlier. The arrangement of the sample in the cell is identical to the cell arrangement for the resistivity studies, except for the fact that the sample is placed vertically in order to take advantage of the natural temperature gradient which exists in the furnace. The entire TEP system is shown in Fig.2.9. The design of the TEP measuring system is centered round the temperature controller.

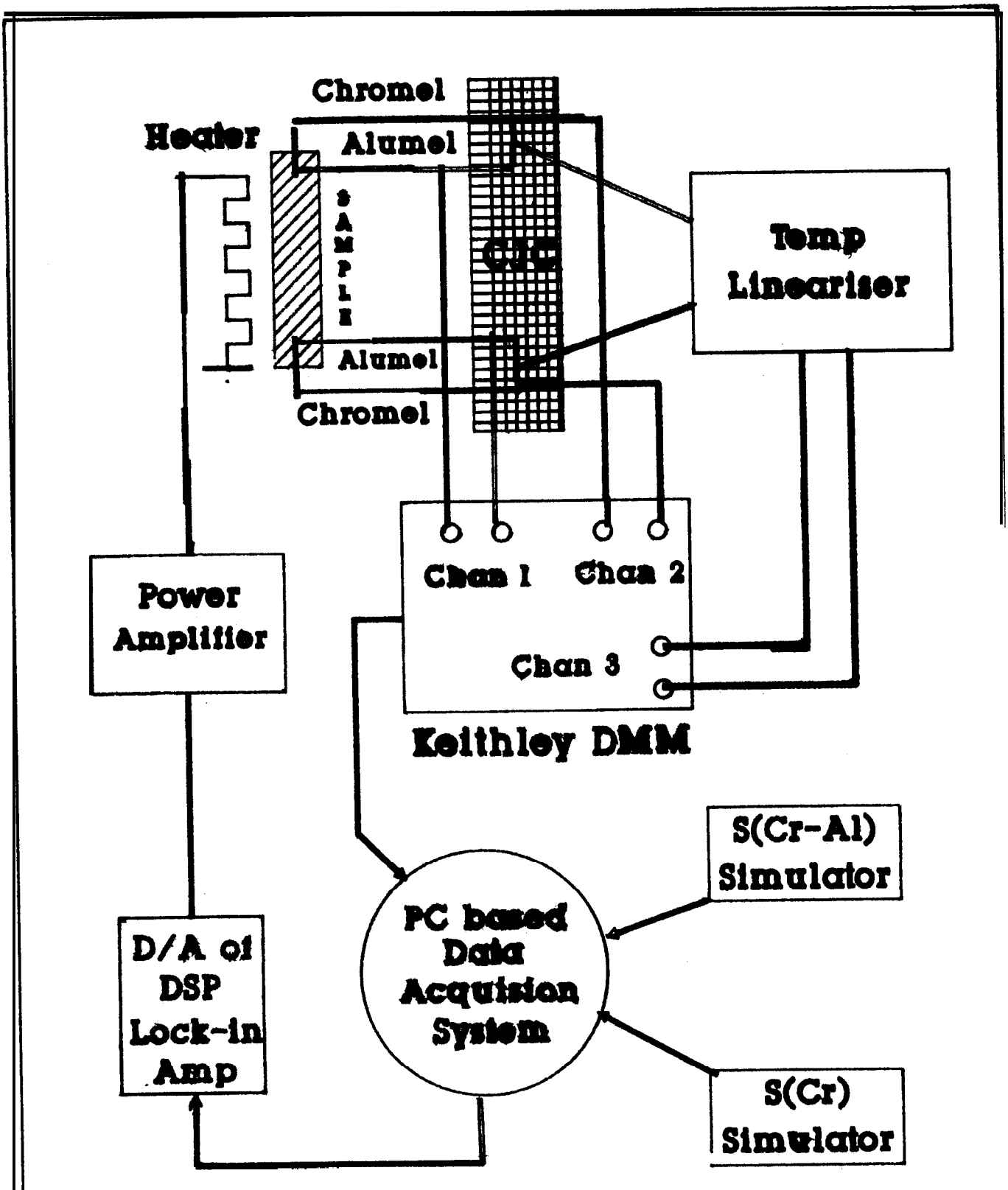

Figure 4.9: TEP measuring system

The temperature control is implemented using a PID algorithm integrated into the software. The D/A (16 bit) of a DSP lock-in amplifier (SRS 830) was used for this purpose. The output of the D/A is fed to the power amplifier which supplies the requisite power to the heater.

An important requisite for TEP measurement is the control of the temperature gradient. The control of the temperature gradient is such that, while the mean temperature T is held constant, the magnitude of the temperature difference ΔT across the ends of the sample can be altered at will.

To calculate the thermo-emf ,S, of the sample, the voltages $V_{chr-sam-chr}$ and $V_{Alu-sam-Alu}$ were measured using a Keithley digital multimeter (DMM). The DMM (model 2001) was interfaced to a personal computer using IEEE 488.2 interface card. The programmes for the interfacing were written in the VIEWDAC environment supplied by Keithley. The VIEWDAC environment allows for real-time plotting of the data.

The absolute TEP, S , of the sample , in the differential mode of measurement ,is given by [9],

$$S(T) = S_{chr}(T) - S_{chr-alu}(T)\left[\frac{V_{chr-sam-chr}}{V_{chr-sam-chr} - V_{alu-sam-alu}}\right] \qquad (2.1)$$

Where S_{chr} and $S_{chr-alu}$ are the absolute thermopower of Chromel and the thermopower of the Chromel-Alumel thermocouples respectively. $V_{chr-sam-chr}$ and $V_{alu-sam-alu}$ are the differential voltages developed across the thermocouples formed out of the reference probes and the specimen, when a small temperature difference is maintained across the length of the sample. In order to evaluate S as a function of temperature, it is necessary to simulate the temperature dependence of both S_{chr} and $S_{chr-alu}$.

Since TEP in the differential mode of measurement is related to the limiting value of the quantity in the square bracket in the expression for S as $AT \rightarrow 0$, the system should have the provision to evaluate this quantity for different AT holding the mean temperature T constant. These requirements have been met by employing two separate controllers for the variables T and AT.

The non-linear variations with temperature of the physical quantities like the absolute TEP of Chromel (S_{chr}) and the relative TEP of Chromel-Alumel thermocouple ($S_{chr-alu}$) are simulated by employing a sixth-order polynomial curve fit

$$S(T)_{chr-alu} = b_o + b_1 T + b_2 T^2 + ...b_6 T^6 \qquad (2.2)$$

$$S(T)_{chr} = c_o + c_1 T + c_2 T^2 + ...c_6 T^6 \tag{2.3}$$

Where $b_o....b_6$ and $c_o.....c_6$ are constants. These constants can be evaluated from computer fit of the NBS data [10].

An algorithm based on the above expressions forms the basis for simulating S_{chr} and $S_{chr-alu}$.

In order to obtain a higher precision in the fit, the temperature range was divided into two blocks namely 0"-200" C and 200^o - 1000" C. The fitting error for $S_{chr-alu}$ in the two ranges are $\pm 0.004^o \mu V/^o$ C and $\pm 0.03 \mu V/^o$ C.

For S_{chr} the fitting errors are $\pm 0.001 \mu V/^o$ C and $\pm 0.1 \mu V/^o$ C on the two ranges.

The overall accuracy of TEP measurement is $\sim$ 0.5% and the resolution is around $\pm 0.01 \mu V/^o$ C.

References

[1] Reshamwala A.S and Ramesh T.G, J.Phys.E (Sci.Instrum), **7,** 133 (1974)

[2] Jayaraman A., Hutson A.R, Mcfee J.H, Coriell A.S and Maines R.G, Rev.Sci.instrum, 38, 44 (1967)

[3] Reshamwala A.S and Ramesh T.G., J.Phys.E (Sci.Instrum)m 8, 465 (1975)

[4] Decker D.L., Bassett W.A., Merrill L., Hall H.T. and Barnett J.P, J.Phys.Chem.ref.data, **1**, 773 (1972)

[5] V.Shubha, *Ph.D* thesis, University of Mysore, 1980

[6] Strong H.M and Bundy F.P , Symposium on accurate characterization of high pressure environment held at National Bureau of Standards, Gaithersburg

[7] Bundy F.P., J.Appl.Phys., **32,** 483, 1961

[8] V.Shubha and T.G.Ramesh, High temp.High Press., 18,311 (1986)

[9] R.D. Barnard in Thermoelectricity in Metals and Alloys, Taylor and Francis LTD, 1972

[10] V.Shubha and T.G.Ramesh, High Temp. High Press., **9,** 461 (1977)